HHS Public Access

Author manuscript

Acta Biomater. Author manuscript; available in PMC 2022 February 01.

Published in final edited form as:

Acta Biomater. 2021 February ; 121: 180–192. doi:10.1016/j.actbio.2020.11.037.

Protein composites from silkworm cocoons as versatile biomaterials

Feng Wang[#†,‡], **Chengchen Guo**[#‡], **Chunmei Li**[‡], **Ping Zhao**[†], **Qingyou Xia**[†,*], **David L. Kaplan**[‡,*]

[†] Biological Science Research Center, Chongqing Key Laboratory of Sericultural Science, Chongqing Engineering and Technology Research Center for Novel Silk Materials, Southwest University, Chongqing, 400715, PR China;

[‡] Department of Biomedical Engineering, Tufts University, Medford, MA, 02155, USA

[#] These authors contributed equally to this work.

Abstract

Silk is a naturally occurring biopolymer formed into fibers composed primarily of fibroin and sericin proteins. The outstanding mechanical properties of silk fibroin (SF) provides numerous applications for silk-based biomaterials. However, canonical approaches for fabricating silk-based biomaterials typically involve degumming to remove the sericin to avoid adverse biological effects. However, sericin also has biological properties that are useful to exploit in new materials, including anti-oxidation and anti-bacterial, inspiring the use of sericin-based biomaterials for biomedical applications including wood healing. However, compared to fibroin, sericin-based materials do not provide robust mechanical properties. To address this problem, we report a method for fabricating fibroin-sericin protein composites into a broad range of materials formats (e.g. films, sponges, monoliths) directly from whole cocoons, negating the traditional extraction step to remove the sericin. This approach combines the material features from both fibroin and sericin, achieving advantages regarding simplified processing and new materials properties. These fibroin-sericin protein composite materials promoted cell adhesion, growth and proliferation and could be fabricated into a variety of materials formats to fit different biomedical applications.

Graphical Abstract

[*] To whom correspondence may be addressed. Xiaqy@swu.edu.cn, David.kaplan@tufts.edu.

Author contributions

F.W., C.G., Q.X., and D.K. designed experiments and the supervised studies. F.W. and C.G. performed the experiments and wrote the original manuscript. F.W., C.G., C.L., P.Z., Q.X., and D.K. edited and revised the manuscript. All authors have given approval to the final version of the manuscript.

Conflict of Interest

The authors declare no conflict of interest.

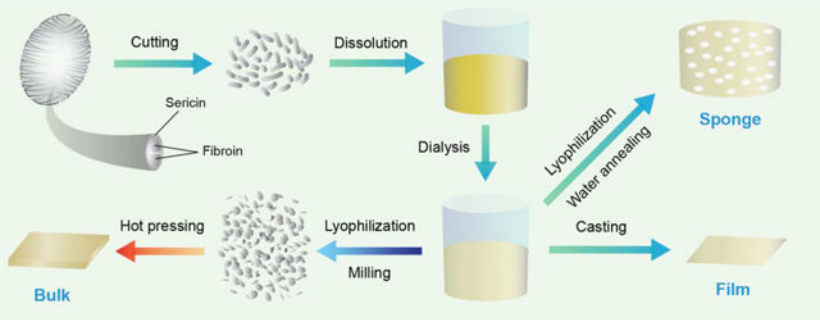

Canonical approaches for fabricating silk-based materials primarily focus on engineering silk fibroin (core structural protein) into different material formats, typically involving degumming to remove the sericin (skin layer) to avoid potential adverse biological effects. Sericin has anti-oxidation and anti-bacterial properties that are useful to exploit in new biomedical materials. Here we provide a novel method for fabricating fibroin-sericin protein composites directly from whole cocoons, with a focus on avoiding current processing steps in the field, while engineering the materials into a variety of materials formats. The results show that different formats of these new fibroin-sericin protein composites can be fabricated (e.g. films, sponges, monoliths) to meet different biomedical application needs.

Keywords

cocoon; silkworm; silk; sericin; composite

1. INTRODUCTION

Silk produced by the silkworm (*e.g. Bombyx mori*) has been redefined in recent years, away from just a traditional textile material and now as a functional biomaterial in biomedical research such as for tissue engineering and regenerative medicine.[1–4] As a protein-based natural material, silk fibers from the raw cocoon are composed of fibroin (~75%) and sericin proteins (~25%) where two parallel fibroin fibers are held together by a layer of sericin on their surfaces.[5–8] The fibroin protein possesses a molecular weight over 400 kDa and serves as structural protein with diverse secondary structures and nano/micro hierarchical structures, responsible for the unusual and remarkable mechanical properties of silk fibers.[9–11] Given these mechanical properties as well as the biocompatibility and biodegradability, SF has emerged with a broad range of utility in silk-based biomaterials.[1, 12–13]

Compared to fibroin, silk sericin (SS) is a mixture of functional proteins primarily encoded by the *sericin-1*, *sericin-2*, and *sericin-3* genes with molecular weights ranging from 20 kDa to 400 kDa.[7, 14–17] Unlike the fibroin proteins, sericin proteins serve as adhesive agents to bind silk fibroins together, thus unlike the fibroins, they are not structurally robust. However, sericin has been reported to offer scientific and commercial value due to its functional attributes as a readily available protein-based biomaterial.[18–20] Some reports have shown that sericin can be used as moisturizing powder for wound healing and stimulating cell proliferation due to its good biocompatibility.[21–22] Further, the antioxidant properties associated with the low digestibility of sericin expands its application in biomedical fields

such as an antimicrobial and anti-inflammatory agent, and in tissue engineering and drug delivery.[18, 23–26]

However, canonical silk processing involves a degumming process to remove the sericin from the cocoons in order to extract the value-added core silk fibroin for downstream processing. Since both the fibroins and sericins possess unique as well as complementary properties with potential in diverse biomedical applications, one intriguing question was raised, “is it possible to combine both types of proteins to fabricate sericin-fibroin (SS-SF) protein composites for biomedical utility, starting from the whole raw cocoon?” Here, strategies were developed to overcome the processing challenges and using whole cocoons directly toward fabricating these new SS-SF protein composites, resulting in the successful formation of versatile biomaterials. Furthermore, biocompatibility and low immunogenicity of these SS-SF protein composite materials was demonstrated. The present work demonstrates the successful fabrication of SS-SF protein composites, effectively shortening the material fabrication process and preserving the native properties of the silk proteins, while also achieving a time and cost-effective process. The approach also provides a promising method to fabricate functional silk-based materials since bioactive molecules, such as growth factors and antibodies, can be co-expressed with fibroin/sericin during the silkworm production process.[27–30] Modern transgenic biotechnology has demonstrated the use of the silkworm as natural bioreactor to express significant quantities of recombinant foreign proteins such as human type III pro-collagen,[31] human serum albumin,[32] human acid fibroblast growth factor,[33] and antibodies [34–35] in the worm native glands along with the synthesis of silk proteins, particularly sericins. These efforts have reshaped ancient silk material into a new versatile biofunctional biomaterials. However, to date, efficient protein expression systems have been demonstrated with the sericin-related encoded genes in *B. mori*,[27–29, 36–37] but only with limited success with fibroin.[38] The new approach demonstrated in this work would be a path forward to utilize genetically modified silk materials with co-expressed functional biomolecules, tailored into various material formats with multi-functions for different biomedical applications. Thus, this would be essentially a one step process from raw cocoon to functionalized medical materials with selective functions.

2. EXPERIMENTAL SECTION

2.1. Cell lines and cell culture

Human skin fibroblast cell line BJ (ATCC® CRL-2522™), and mouse macrophage cell line RAW 264.7 were commercially purchased (ATCC, USA) and cultured in Dulbecco’s modified Eagle’s media (DMEM, Gibco), supplied with 10% (v/v) fetal bovine serum (FBS, Gibco) and 100 units/mL of penicillin, 100 μg/mL of streptomycin, and 0.25 μg/mL of Gibco Amphotericin B (Gibco® Antibiotic-Antimycotic-100X, Thermofisher Scientific) at 37ºC at 95% air and 5% CO_2. Commercially purchased mouse bone marrow-derived MSCs (ATCC, USA) within five passages were maintained in our lab and cultured in mesenchymal stem cell basal medium (ATCC®PCS-500-030™, USA) supplied with a mesenchymal stem cell growth kit (ATCC®PCS-500-041™, USA) and 100 units/mL of penicillin, 100 μg/mL

of streptomycin, and 0.25 μg/mL of Gibco Amphotericin B (Gibco® Antibiotic-Antimycotic-100X, Thermofisher Scientific) at 37ºC at 95% air and 5% CO_2.

2.2. Preparation of SS-SF aqueous solution using whole cocoons

After removal of the pupa, the cocoons were frozen first in liquid nitrogen and then crushed into powder with an analytical mill (IKA, Staufen, Germany). The cocoon powders were then dissolved in the 9.3 M LiBr solution (Sigma-Aldrich, USA) with a concentration of 5% (w/v) at 60°C for 4–6 hrs. The dissolved silk solution was centrifuged at 9,000×*g* for 20 min at room temperature, the undissolved residues were discarded and the liquid supernatant was collected and dialyzed (cellulose dialysis membranes, MWCO 3,500 Da, Spectrum Laboratory, Inc, USA) against deionized water at room temperature for 3 days with at least six changes of the DI water to completely remove the salts. The insoluble residues in the dialysis membranes were discarded by centrifugation at 9,000×*g* for 20 min at room temperature. The aqueous whole silk solutions were then transferred into 50 ml-centrifuge tubes and stored at 4 °C before use. The concentration of the whole silk in solution (w/v) was determined by dividing the weight of the dry silk to its initial volume.

2.3. Fabrication of SS-SF films 3D-sponges and bulk materials

A 5 mL aliquot of 2 % (wt/vol) aqueous SS-SF solution was cast onto a 100 mm polystyrene petri dish surface and allowed to dry overnight without covering the dish in a fume hood at room temperature. The dried SS-SF films were water annealed by placing the films in a temperature-controlled water vapor annealing device with vacuum pressure of −25 in Hg (−85 KPa), distilled water and room temperature for 12 h to induced the formation of β-sheet and crystallization in the silk proteins to prevent the films from dissolving in water. [39] Afterward, the samples were taken out periodically for further measurements. To fabricate SS-SF 3D porous sponges, each 1 mL of 2% (wt/vol) aqueous SS-SF solution was poured into each well of a 48-well plate. The plate was then covered and frozen overnight at −20 °C and lyophilized for 3 days. Thereafter, the plate was placed into the temperature-controlled water vapor annealing device to induced formation of β-sheet and crystallization of the silk proteins to prevent the sponges from dissolving in water. [39] Fabrication of the SS-SF bulk materials was by thermal processing.[40] The 2 % (wt/vol) aqueous SS-SF solution was rapidly frozen in liquid nitrogen for 15 minutes and then lyophilized for 3 days. The dried SS-SF sponges were collected and milled into powder using an analytical mill (IKA, Staufen, Germany). The solid-state SS-SF powders were packed into predesigned molds, followed by hot pressing at 632 MPa and 145 °C for 15 min. SS-SF bone screws (outer diameter ~1.8 mm, pitch 600 μm) were machined from SS-SF bars on a CNC lathe (Trak TRL 1440 EX, Southwestern Industries). A custom single point external cutter (Vargud) was used to cut screw threads by matching the turning speed with the horizontal speed of the cutter to cut a desired pitch length. The screw heads were machined to have a cylindrical head, and a slot was generated.

2.4. Scanning electron microscopy (SEM)

All samples were frozen in liquid nitrogen for 5 min and lyophilized prior to SEM observation. Then the samples were vacuum-coated with a layer of platinum (NeoCoater MP-19020NCTR, Jeol, Japan) and imaged by SEM (JSM-5610LV, JEOL, Japan) at 5 kV.

2.5. Fourier Transform Infrared Spectroscopy (FTIR) analysis

Secondary structures of SS-SF samples were assessed by a Fourier transform infrared spectroscopy (Jasco FTIR-6200, Jasco Instruments, Easton, MD) over a spectral region of 4000–650 cm^{-1} with a 4 cm^{-1} nominal resolution. Deconvolution of amide I bands in spectra was performed using the Omnic, PeakFit v4.12 software. The second derivative spectra from peak numbers and positions were utilized during the deconvolution. The band shape and the bandwidth were calculated in a Gaussian model. Each spectrum represented the result from a single test, while the data for each sample (e.g., β-sheet content) was the average of at least three independent deconvolutions from different samples.

2.6. Mechanical properties

Mechanical testing was carried out on an Instron 3366 machine (Instron, Norwood, US) equipped with a load cell of 50 N at 25 °C and 50% relative humidity. For unconfined compression, the SS-SF 3D sponges with 8 mm in height and 12 mm in diameter were placed on a metal plate coated in a tank full with PBS to keep the sponges hydrated, and each sample was tested with a loading velocity of 1 mm/min and repeated at least three times. Three-point bending was applied for the mechanical testing of the SS-SF hard plates. The plate pieces (7 mm width, 12 mm length, 1 mm thick) were placed on the Instron 3366 machine (Instron, Norwood, US) equipped with a support interval of 10 mm and a testing speed of 1 mm/min. The bending strength and elastic modulus of the samples were calculated from the stress-strain curves. The maximum failure strength was calculated from the average of at least three independent measurements.

2.7. Wide-angle X-ray scattering

The degree of crystallinity of the SS-SF materials was determined by the wide-angle X-ray scattering on the BioCars 14BM-C beamline at the Advanced Photon Source at Argonne National Laboratory (city, state). Tests were performed with a fixed energy of 12.668 keV, a wavelength of 0.979 Å for the X-ray beam, and beam size of 150 × 300 μm (horizontal × vertical) on the sample. Data were recorded by an ADSC Quantum 315r detector. CeO_2 powder was used for instrument calibration. The 2D wide-angle X-ray diffraction patterns were analyzed using the software package FIT2D.

2.8. Porosity

The dry SS-SF 3D sponges or hard plates were immersed in a known volume (*v1*) of water in a graduated cylinder. Two-hours after the sponge or hard plate fully absorbed the water, the total volume (including water and the scaffold or the hard plate) was recorded as *v2*. The volume of the water remaining in the cylinder after the removal of the scaffold or hard plate was recorded as *v3*. The porosity (%) of the scaffold or plate was obtained by:

$$\text{Porosity}\left(\%\right) = \frac{v1 - v3}{v2 - v3} \times 100$$

2.9. Water uptake

The dry SS-SF samples (mass is marked as W_1) were immersed in 1×PBS, pH 7.4. At different time points, the swollen samples were removed to determine the weight as W_2. The water uptake of the samples was calculated using the following equation:

$$\text{Water uptake}\left(\%\right) = \frac{W2 - W1}{W2} \times 100$$

2.10. In vitro degradation

Dry SS-SF 3D sponges or bulk plates with a weight of 100 mg were incubated in 1 mL of 1×PBS (pH 7.4) with or without 3.1 U/mL protease XIV, an enzyme which degrades β-sheet crystallized silk samples at 37°C.[41] The PBS with or without (control) the protease XIV was replaced every two days. At different time points, samples were removed, dried and weighed. Samples for each time point were run in triplicates.

2.11. In vitro inflammatory responses assay

The *in vitro* cell responses to the SS-SF materials were assessed using macrophages RAW264.7 (TIB-71, ATCC, Manassas, VA, USA). SS-SF film discs or fibroin film discs with 8 mms diameter sterilized by UV radiation for 30 min, conditioned with Dulbecco's modified eagle medium (DMEM) for 6 h before cell seeding in 96 well plates. Aliquots (100 μL, 1×10^4 cells) of RAW264.7 suspensions at ~90% confluence were seeded on the surfaces of the SS-SF films or fibroin films. Meanwhile, equal amounts of RAW264.7 cells were seeding directly into the wells of 96-well plates without films with or without lipopolysaccharide (LPS) at doses of 5 μg/mL as positive or negative controls, respectively. Cells were then cultivated in DMEM with 10% (w/v) FBS at 37°C and 5% CO_2. At days 1 and 7 post cell seeding, the cell medium supernatants were collected for quantitation of TNF-α and IL-2 release using an TNF alpha Mouse ELISA Kit (Thermo Fisher Scientific, USA) and IL-10 Mouse Uncoated ELISA Kit (Thermo Fisher Scientific, USA) according to the instructions of the manufacturer.

2.12. Cell seeding on the SS-SF films, porous 3D sponges and bulk plates

For cell seeding on the SS-SF films and dense plates, punched films or hard plate discs with 8 mm in diameter were placed into 96-well plates and sterilized by UV radiation for 30 min. The samples were then conditioned with Dulbecco's modified eagle medium (DMEM) for 6 h before cell seeding. Then ~96% confluent human fibroblast BJ cells (ATCC® CRL-2522™) were suspended in fresh complete culture media with 10% FBS and seeded on the surfaces of the SS-SF films at 1×10^3 cells per 100 μL volume per well. The cells were cultured at 37°C at 95% O_2 and 5% CO_2; fresh complete culture media with 10% FBS was replaced every three days. For cell seeding on the porous 3D SS-SF sponges, the silk sponges were cut into disks with 8 mm in diameter and 2 mm in thickness using a biopsy punch, sterilized in 70% ethanol for 30 min, washed by PBS five times to completely remove the ethanol, and subsequently allowed to condition in 24 well plates with complete cell culture media for 6 h at 37°C. The ~96% confluent human fibroblast BJ cells (ATCC® CRL-2522™) or mouse bone marrow-derived MSCs were seeded on each porous 3D SS-SF

sponge disk at a density of 30,000 cells/cm^2 and allowed to adhere for 30 min prior to flooding with media for cultivation in an incubator maintained at 37°C and 5% CO_2. The plates were replaced with fresh cell culture media every three days.

2.13. AlamarBlue assay

The long-term cell viability of the cells was determined by AlamarBlue assay (Thermo fisher Scientific, USA) according to instruction. At each time point post seeding, 1/10th volume of the AlamarBlue reagents were added directly into the culture media with the silk samples and cells, and then incubated at 37°C with 5% CO_2 for 4 h. Thereafter, aliquots (100 μL) were aspirated into a new black 96 well plate for quantification using a fluorescence plate reader (ex/em ~560 nm/~590 nm). Cells plated in tissue culture wells (TCP) were maintained as above and utilized as controls, while wells of the TCP without cells were used to adjust for background fluorescence.

2.14. Live/Dead Cell staining

Cell viability on the surface of the different SS-SF materials or TCP plates (controls) at different times after seeding were estimated using a LIVE/DEAD® Viability/Cytotoxicity Kit (Thermo fisher Scientific, USA). Briefly, at each detection time point, cells seeded on the different SS-SF materials were incubated with calcein AM and ethidium homodimer-1 (EthD-1) for 30 min and protected from light to stain live (green) and dead cells (red), respectively. Then, cells were imaged using a BZ-X700 series microscope (Keyence, Itasca, IL) with excitation at 488 nm and emission at 515 nm for live cells and excitation at 570 and emission at 602 nm for dead cells. Cells seeded on the porous 3D SS-SF sponges were imaged using confocal laser scanning microscopy (Leica FLIM SP8, Wetzlar, Germany) with an imaging filter set for live cells (Ex/Em: 488/515 nm) and dead cells (Ex/Em: 570/602 nm). 3D rendering images and confocal 3D maximum projection images were assembled with Leica confocal software (LAS X version: 3.4.2.18368).

2.15. Immunofluorescence

Cell viability and morphology seeded on the 3D SS-SF sponges were investigated by F-Actin filament and DAPI staining. Briefly, cells within the sponges were fixed with 3.7% methanol-free formaldehyde (Thermo fisher Scientific, USA) in PBS for 15 minutes at room temperature, permeabilized with 0.1% Triton® X-100 for 15 minutes at room temperature, blocked by 1% BSA for 45 min at room temperature, and further stained by Rhodamine Phalloidin (Thermo fisher Scientific, USA) and DAPI (Thermo fisher Scientific, USA) for additional 60 minutes at room temperature. Finally, the cells were visualized using confocal laser scanning microscopy (Leica FLIM SP8, Wetzlar, Germany) with an imaging filter set specific for F-Actin filaments dye (Ex/Em: 540/565 nm) and cell nucleus dye (Ex/Em: 358/461 nm). 3D rendering images and confocal 3D maximum projection images were assembled with Leica confocal software (LAS X version: 3.4.2.18368).

2.16. Cell proliferation by EdU incorporation

Cell proliferation (fibroblast BJ cells or MSCs) in the 3D SS-SF sponges were measured using Click-iT® EdU Imaging Kits (Thermo Fisher Scientific, USA). Briefly, 24 h after

cultivation, the cells seeded on the 3D SS-SF sponges were labeled with EdU (5-ethynyl-2'-deoxyuridine, a nucleoside analog of thymidine) at a concentration of 10 μM at 37°C overnight. Then, labeled cells were fixed with 3.7% methanol-free formaldehyde in PBS for 15 minutes at room temperature and permeabilized with 0.5% Triton® X-100 for 20 minutes at room temperature. This process was followed by EdU detection by Alexa Fluor®555 picolylazide and nuclear staining by Hoechst®33342 dye for 30 minutes at room temperature. Cell were visualized by confocal laser scanning microscopy (Leica FLIM SP8, Wetzlar, Germany) with an imaging filter set specific for Alexa Fluor®555 picolylazide (Ex/Em: 555/565 nm) for proliferating cells and cell nuclei (Ex/Em: 358/461 nm). 3D rendered images and confocal 3D maximum projection images were assembled with Leica confocal software (LAS X version: 3.4.2.18368).

2.17. Statistical Analysis

All measurements were performed in triplicate and repeated independently three times. Data are indicated as mean ±S.D. (standard deviation) for at least n=3. Statistical analyses were calculated by Student's *t*-test. *$p < 0.05$ was considered statistically significant, **$p < 0.01$ was considered highly significant and ***$p < 0.001$ was considered extremely significant. Details on the experimental methods can be found in Supporting Information.

3. RESULTS AND DISCUSSION

3.1. Fabrication of SS-SF materials from raw cocoons

Here, we considered both the fibroin and sericin for materials fabrication. A schematic of the typical strategy and processing route used in this study is shown in Fig. 1A. Initially, the natural cocoons were frozen using liquid nitrogen and milled into powders. The powders were then dissolved in 9.3 M lithium bromide (LiBr), commonly used solvent for dissolving degummed silk fibroins [42] to obtain a homogenous SS-SF aqueous solution. Several previous studies reported that higher sericin concentrations could reduce the solubility of sericin in water and accelerate conversion of random coil structures into β-sheets, resulting in gelation [25]. To prevent gelation of the SS-SF solution during dialysis to achieve longer-term storage, the dissolution of the raw silk powders in the LiBr was conducted at an initial concentration of 5% (w/v), where complete dissolution of the cocoon powders was observed, yielding a homologous SS-SF aqueous solution with final concentration of 2% (w/v) after dialysis and purification. These homologous SS-SF aqueous solutions were stable at 4 °C for as long as two months without gelation, suggesting the sericin concentration around 0.4–0.6% (w/v). In contrast, SS-SF solutions prepared with a higher starting concentration were unstable and formed gels during dialysis or during storage. Accordingly, the initial concentrations of raw silk used in subsequent preparations was 5% w/v.

The molecular weights of the silk proteins in the SS-SF aqueous solution dissolved from the raw silk were analyzed and compared with those in fibroin aqueous solutions dissolved from 30 min extracted degummed silk. SDS-PAGE showed that the sericin and fibroin dissolved directly from the raw silk were concentrated at the higher molecular weight (MW) markers around 400 kDa, while the SF dissolved from the degummed silk was found at the lower molecular weight range from 30–268 kDa and with a broad range, as expected (Fig. S1A).

The degumming process during cocoon processing is well known to result in the degradation of fibroin chains,[43–44] whereas the direct dissolution of the raw silk without degumming avoided the degradation, possibly providing benefits to the physical and biological properties of silk materials fabricated from these proteins.[45] The resultant homogenous SS-SF aqueous solutions can be utilized directly to generate SS-SF composite materials in various formats, including films and three dimensional (3D) sponges.[42] In addition, the solution can be freeze-dried, then subjected to hot-pressing to generate bulk materials (e.g., bars, discs) and devices (e.g., screw) with machining following a thermal processing method.[40] Images of materials fabricated from SS-SF are presented in Fig. 1B, demonstrating the fine properties, freestanding robust properties and the absence of cracks.

3.2. Physical characterization and in vitro cytocompatibility of SS-SF films

Fabrication of SS-SF films was accomplished by direct casting of the 2% (w/v) SS-SF aqueous solution followed by water annealing to drive crystallization and insolubility.[39] These SS-SF films were optically transparent, rough and flexible (Fig. 2A). Fourier transform infrared (FTIR) spectroscopy was used to assess β-sheet content in the dry SS-SF films and the results indicated that the water annealing induced a conformational transition of the amorphous silk proteins in the fibroin-sericin films from random coil structures (1645 cm^{-1} in FTIR) to β-sheet (1621 cm^{-1} in FTIR) (Fig. S1B and C). Deconvolution of the amide I band region (1590–1699 cm^{-1}) [46] provided an estimated percentage of β-sheets in the films of 46.8±1.0% (n=30) (Fig. S1D). The morphology of the SS-SF films was characterized by SEM (Fig. 2B and C); the surface was macroscopically smooth and the thickness of the films was 1.2±0.4 μm (n=10). Cellular responses are critical for a biomaterial and sericin has been explored for new biomaterial applications,[18, 23, 25, 47] while also a challenge due to potential inflammatory responses *in vitro* and in combination sericin with fibroin.[48–49] Thus, the cellular response to the SS-SF films was assessed using macrophage RAW 264.7 cells exposed to the SS-SF films and controls (SF, TCP, LPS) for a week. At day 1 post seeding, the RAW 264.7 cells had a round morphology and adhered well on the SS-SF film surfaces (Fig. 2G), similar to the response on the SF films (Fig. 2F) and the TCP (Fig. 2D). In contrast, RAW 264.7 cells seeded on the TCP with LPS treatment underwent morphological transformation from macrophage-like morphology into distinct dendritic-like morphology with larger cell size and cytoplasm with increased granularity (Fig. 2E).[50] Here, the areas and diameters of the cells seeded on SS-SF film surfaces were similar with those seeded on the SF films and TCP surfaces, and significantly smaller compared to those on the TCP-LPS induced RAW 264.7 cells (Fig. 2H and I). The release of early indicators of inflammation, interleukin-10 (IL-10) and tumour necrosis factor-α (TNF-α) at days 1 and 7 was detected and similar to these cells seeded on the SF films and TCP plates, while significantly lower compared to the LPS group (Fig. 2J and K), suggesting the sericin present in the SS-SF films caused no significant cell inflammatory responses in vitro. This could be ascribed to the processing method by directly dissolving silk fibers without degumming, thus retaining the natural molecular weights of sericin and fibroin proteins (Fig. S1A).

The viability of human fibroblast BJ cells seeded on the SS-SF films was analyzed by Live/Dead staining, compared to the cells seeded on TCP plate controls (Fig. 2L and 2N). Most of

the BJ cells seeded on the SS-SF films stained with green fluorescent signals (Fig. 2M), with few cells with red fluorescent signals (Fig. 2N) after culture for 3 days. During cell culture, the BJ cells adhered and grew well on the SS-SF films comparable to that on the TCP (Fig. S1E and F). Additionally, BJ cells grew with a fibroblast-like morphologies and formed monolayers, which were comparable to the cells grown on the TCP plate (Fig. 2L and M). Unexpectedly, the cells grew significantly better on the sericin-free fibroin films (Fig. S2).

3.3. Fabrication and characterization of 3D porous SS-SF sponges

3D porous SS-SF sponges were prepared following a freeze-drying process.[51] The 2% (w/v) SS-SF aqueous solution was placed into desired molds, freezing-dried, and then treated by water annealing [39] (Fig. S3). Fig. 3A shows photographs of a preformed 2% (w/v) SS-SF sponge in dry and wet states. The SS-SF sponges when dry condition present a uniform morphology (Fig. S4A and B). In addition, the 2% (w/v) sponges also maintained morphology after the rapid and complete water uptake within 2 hours, with a maximum swelling of ~32.9-fold (Fig. 3A and Fig. S4C), indicating that the presence of the hydrophilic sericin component facilitated this water uptake in comparison to silk fibroin alone sponges. SEMs showed the SS-SF sponges possessed typical lamellar, homogeneous and interconnected porous structures with pore sizes of 123.0±28.3 μm and a high porosity of 90.9±1.4% (Fig. 3B and C). The pore sizes of the SS-SF sponges can be adjusted to using a salt leaching method.[42] The SS-SF sponges when hydrated demonstrated ductility and structural integrity, with complete recovery under cyclic compression of over 99% of the original length (Fig. 3D and Movie S1). Furthermore, structural collapse of the wet SS-SF sponges occurred while blotting water from sponge, with full recovery immediately upon reabsorption of water within seconds (Movie S2 and 3). FTIR characterization observed significant conformational transition of the silk proteins in these SS-SF sponges, from random coil to β-sheet after water annealing treatment (Fig. 3E). The deconvolution of the amide I band revealed a β-sheets content of ~24.7±0.6%. The mechanical properties of the wet SS-SF sponges were characterized by compression tests in PBS (Fig. 3F). The compressive modulus of the SS-SF sponges was 3.0±1.3 kPa at 20% compressive strain, demonstrating shape recovery and fatigue resistance after the cyclic compression.

The biological properties of the SS-SF sponges were evaluated with the cultivation of mesenchymal stem cells (MSCs). Cellular growth was imaged by 3D scanning 100 μm depths from the top of the sponge using confocal microscopy (Fig. 4A). The MSCs grew on the surface of the SS-SF sponges and occupied the space in the interconnected pores to form a compact mat of cells with distinct rounded nuclei and well-developed actin filaments manner (Fig. 4B and Fig. S5). Notably, scanning deeper than 100 μm showed MSCs with distinct nuclei and filaments were also observed to grow both horizontally and migrate vertically in the sponges (Fig. 4C and D and Movie S4), suggesting efficient penetration of MSCs within the porous structure of the 3D SS-SF sponges. Viability of MSCs in the SS-SF sponges two weeks post seeding was imaged by confocal microscopy and showed dominance by >95% live cells and few dead cell fluorescence signals (Fig. 4E), indicating an absence of cytotoxicity of the SS-SF sponge. EdU incorporation [52] reflecting cell proliferation showed that most of the MSCs were proliferative within the SS-SF sponges over two weeks (Fig. 4F-H). This response can be explained by the cell adhesive features of

sericin.[22–23, 53] In addition, monitoring cell viability by alamarBlue for two weeks revealed continuous cell growth of the MSCs within the SS-SF sponges (Fig. 4I), suggesting longer-term cell survival and proliferation. Similar results related to the growth and efficient penetration of MSCs in the SS-SF sponges was also observed with fibroblasts (Fig. S6), suggesting the overall cytocompatibility of the sponges.

3.4. Fabrication of bulk SS-SF materials and devices

We recently developed a thermal processing method involving direct thermal molding of solid regenerated silk fibroin into new material formats with tailored properties and functionalities.[1, 40] This method significantly shortened the steps of silk canonical processing. Here, the feasibility of fabricating SS-SF bulk materials by direct thermoplastic molding of regenerated SS-SF solid powder was assessed. The aqueous regenerated SS-SF solution (~2%, w/v) was freezing-dried and milled to obtain solid stated SS-SF powder as the raw material (Fig. S7A). Hot-pressing processing under 632 MPa and 145 °C was utilized, [40] to pack the SS-SF powder in a predesigned mold to form dense bars and discs with a pale yellow and transparent appearance (Fig. 1B and Fig. S7B), indicating successful thermal treatment. These bulk SS-SF bars could be machined into medical devices such as bone screws (Fig. 5A). Surface scanning electron microscopy (SEM) images showed that the SS-SF-based bone screws had a homologous structure after the hot pressing (Fig. 5B-D). FTIR characterization identified significant β-sheet structure (~44.7%) (Fig. 5E). In addition, Wide-angle X-ray scattering (WAXS) showed that the solid-stated SS-SF powder possessed significantly different molecular structure compared to the hot pressed SS-SF screws, indicating a structural transition to silk II (scattering vector q = 14.6 nm^{-1}, d-spacing value of 4.3Å) during the processing (Fig. S8). The mechanical properties of these materials were evaluated by three-point bending of SS-SF plates and showed a maximum strength of ~116±8.5 MPa (Fig. 5F). In vitro water uptake in PBS at 37°C showed that the fabricated SS-SF bone screws had a water uptake within 6 h with a maximum swelling of ~30 wt% (Fig. 5G and Fig. S9), likely due to the presence of the hydrophilic sericin in the SS-SF bone screws. The SS-SF bulk materials were also nontoxic, biodegradable and cytocompatible, and the SS-SF plates supported cell adhesion, survival and growth comparable to TCP (Fig. 5H-I and Fig. S10).

4. CONCLUSIONS

A novel method to fabricate versatile SS-SF protein composites in a variety of material formats, including films, sponges, and bulk devices, was demonstrated through aqueous regenerated protein solution or solid-state processing techniques. This method involved directly dissolving whole raw silk cocoons without degumming, which simplifies the processing steps for silk materials fabrication and achieves improved processing costs, while avoiding the degradation of the fibroin proteins. The sericin present in these SS-SF materials did cause an in vitro inflammatory response. These SS-SF materials supported cell adhesion, growth and proliferation, thus offering potential utility as biomaterials. This new method may also pose a need for high quality silkworm cocoons to minimize the need to clean debris or contaminants from individual cocoons in order to avoid or minimize downstream issues.

Supplementary Material

Refer to Web version on PubMed Central for supplementary material.

ACKNOWLEDGEMENTS

This work was supported by the NIH (P41EB027062, R01AR068048), the NNSF of China (31530071) and China Scholarship Council (CSC, 201806995035).

REFERENCE:

(1). Li C; Guo C; Fitzpatrick V; Ibrahim A; Zwierstra MJ; Hanna P; Lechtig A; Nazarian A; Lin SJ; Kaplan DL Design of biodegradable, implantable devices towards clinical translation. Nature Reviews Materials 2020, 5 (1), 61–81, DOI: 10.1038/s41578-019-0150-z.

(2). Holland C; Numata K; Rnjak-Kovacina J; Seib FP The Biomedical Use of Silk: Past, Present, Future. Adv Healthc Mater 2019, 8 (1), e1800465, DOI: 10.1002/adhm.201800465. [PubMed: 30238637]

(3). Farokhi M; Mottaghitalab F; Fatahi Y; Khademhosseini A; Kaplan DL Overview of Silk Fibroin Use in Wound Dressings. Trends Biotechnol 2018, 36 (9), 907–922, DOI: 10.1016/j.tibtech.2018.04.004. [PubMed: 29764691]

(4). Ling S; Kaplan DL; Buehler MJ Nanofibrils in nature and materials engineering. Nature Reviews Materials 2018, 3, 18016, DOI: 10.1038/natrevmats.2018.16.

(5). Craig CL Evolution of arthropod silks. Annu Rev Entomol 1997, 42, 231–67, DOI: 10.1146/annurev.ento.42.1.231. [PubMed: 15012314]

(6). Yamaguchi K; Kikuchi Y; Takagi T; Kikuchi A; Oyama F; Shimura K; Mizuno S. Primary structure of the silk fibroin light chain determined by cDNA sequencing and peptide analysis. J Mol Biol 1989, 210 (1), 127–39, DOI: 0022–2836(89)90295–7 [pii]. [PubMed: 2585514]

(7). Okamoto H; Ishikawa E; Suzuki Y. Structural analysis of sericin genes. Homologies with fibroin gene in the 5' flanking nucleotide sequences. J Biol Chem 1982, 257 (24), 15192–9. [PubMed: 6294094]

(8). Tanaka K; Inoue S; Mizuno S. Hydrophobic interaction of P25, containing Asn-linked oligosaccharide chains, with the H-L complex of silk fibroin produced by Bombyx mori. Insect Biochem Mol Biol 1999, 29 (3), 269–76, DOI: S0965174898001350 [pii]. [PubMed: 10319440]

(9). Jin HJ; Kaplan DL Mechanism of silk processing in insects and spiders. Nature 2003, 424 (6952), 1057–61, DOI: 10.1038/nature01809. [PubMed: 12944968]

(10). Vollrath F; Knight DP Liquid crystalline spinning of spider silk. Nature 2001, 410 (6828), 541–8, DOI: 10.1038/35069000. [PubMed: 11279484]

(11). Zhong J; Liu Y; Ren J; Tang Y; Qi Z; Zhou X; Chen X; Shao Z; Chen M; Kaplan DL; Ling S. Understanding Secondary Structures of Silk Materials via Micro- and Nano-Infrared Spectroscopies. ACS Biomaterials Science & Engineering 2019, 5 (7), 3161–3183, DOI: 10.1021/acsbiomaterials.9b00305. [PubMed: 33405510]

(12). Altman GH; Diaz F; Jakuba C; Calabro T; Horan RL; Chen J; Lu H; Richmond J; Kaplan DL Silk-based biomaterials. Biomaterials 2003, 24 (3), 401–16, DOI: S0142961202003538 [pii]. [PubMed: 12423595]

(13). Asakura T; Tanaka T; Tanaka R. Advanced Silk Fibroin Biomaterials and Application to Small-Diameter Silk Vascular Grafts. ACS Biomaterials Science & Engineering 2019, 5 (11), 5561–5577, DOI: 10.1021/acsbiomaterials.8b01482. [PubMed: 33405687]

(14). Garel A; Deleage G; Prudhomme JC Structure and organization of the Bombyx mori sericin 1 gene and of the sericins 1 deduced from the sequence of the Ser 1B cDNA. Insect Biochem Mol Biol 1997, 27 (5), 469–77. [PubMed: 9219370]

(15). Takasu Y; Yamada H; Tamura T; Sezutsu H; Mita K; Tsubouchi K. Identification and characterization of a novel sericin gene expressed in the anterior middle silk gland of the silkworm Bombyx mori. Insect Biochem Mol Biol 2007, 37 (11), 1234–40, DOI: S0965-1748(07)00187-7 [pii] 10.1016/j.ibmb.2007.07.009. [PubMed: 17916509]

(16). Michaille JJ; Garel A; Prudhomme JC Cloning and characterization of the highly polymorphic Ser2 gene of Bombyx mori. Gene 1990, 86 (2), 177–84. [PubMed: 2323571]

(17). Takasu Y; Yamada H; Tsubouchi K. Isolation of three main sericin components from the cocoon of the silkworm, Bombyx mori. Biosci Biotechnol Biochem 2002, 66 (12), 2715–8. [PubMed: 12596874]

(18). Ahsan F; Ansari TM; Usmani S; Bagga P. An Insight on Silk Protein Sericin: From Processing to Biomedical Application. Drug Res (Stuttg) 2018, 68 (6), 317–327, DOI: 10.1055/s-0043-121464. [PubMed: 29132177]

(19). Lallepak Lamboni MG, Guang Yang, Qun Wang. Silk sericin: A versatile material for tissue engineering and drug delivery. Biotechnology Advances 2015, 33, 1855–1867. [PubMed: 26523781]

(20). Kurland NE; Dey T; Wang C; Kundu SC; Yadavalli VK Silk protein lithography as a route to fabricate sericin microarchitectures. Adv Mater 2014, 26 (26), 4431–7, DOI: 10.1002/adma.201400777. [PubMed: 24737390]

(21). Aramwit P; Kanokpanont S; De-Eknamkul W; Srichana T. Monitoring of inflammatory mediators induced by silk sericin. J Biosci Bioeng 2009, 107 (5), 556–61, DOI: 10.1016/j.jbiosc.2008.12.012 S1389–1723(08)00158–8 [pii]. [PubMed: 19393558]

(22). Aramwit P; Palapinyo S; Srichana T; Chottanapund S; Muangman P. Silk sericin ameliorates wound healing and its clinical efficacy in burn wounds. Archives of dermatological research 2013, 305 (7), 585–94, DOI: 10.1007/s00403-013-1371-4. [PubMed: 23748948]

(23). Lamboni L; Gauthier M; Yang G; Wang Q. Silk sericin: A versatile material for tissue engineering and drug delivery. Biotechnol Adv 2015, 33 (8), 1855–67, DOI: 10.1016/j.biotechadv.2015.10.014. [PubMed: 26523781]

(24). Kundu B; Kundu SC Silk sericin/polyacrylamide in situ forming hydrogels for dermal reconstruction. Biomaterials 2012, 33 (30), 7456–67, DOI: 10.1016/j.biomaterials.2012.06.091 S0142–9612(12)00756–9 [pii]. [PubMed: 22819495]

(25). Kunz RI; Brancalhao RM; Ribeiro LF; Natali MR Silkworm Sericin: Properties and Biomedical Applications. Biomed Res Int 2016, 2016, 8175701, DOI: 10.1155/2016/8175701. [PubMed: 27965981]

(26). Chen CS; Zeng F; Xiao X; Wang Z; Li XL; Tan RW; Liu WQ; Zhang YS; She ZD; Li SJ Three-Dimensionally Printed Silk-Sericin-Based Hydrogel Scaffold: A Promising Visualized Dressing Material for Real-Time Monitoring of Wounds. ACS Appl Mater Interfaces 2018, 10 (40), 33879–33890, DOI: 10.1021/acsami.8b10072. [PubMed: 30204403]

(27). Wang F; Xu H; Wang Y; Wang R; Yuan L; Ding H; Song C; Ma S; Peng Z; Zhao P; Xia Q. Advanced silk material spun by a transgenic silkworm promotes cell proliferation for biomedical application. Acta Biomater 2014, 10 (12), 4947–55, DOI: 10.1016/j.actbio.2014.06.031 S1742–7061(14)00287–6 [pii]. [PubMed: 24980060]

(28). Wang Y; Xu S; Wang R; Chen W; Hou K; Tian C; Ji Y; Yang Q; Yu L; Lu Z; Zhao P; Xia Q; Wang F. Genetic fabrication of functional silk mats with improved cell proliferation activity for medical applications. Biomaterials Science 2019, DOI: 10.1039/C9BM01285K.

(29). Wang F; Wang Y; Tian C; Xu S; Wang R; Hou K; Chen W; Zhao P; Yu L; Lu Z; Kaplan DL; Xia Q. Fabrication of the FGF1-functionalized sericin hydrogels with cell proliferation activity for biomedical application using genetically engineered Bombyx mori (B. mori) silk. Acta Biomater 2018, 79, 239–252, DOI: 10.1016/j.actbio.2018.08.031. [PubMed: 30149211]

(30). Gao X; Qu H; Gao Z; Zeng D; Wang J; Baranenko D; Li Y; Lu W. Protective effects of Ulva pertusa polysaccharide and polysaccharideiron (III) complex on cyclophosphamide induced immunosuppression in mice. Int J Biol Macromol 2019, 133, 911–919, DOI: 10.1016/j.ijbiomac.2019.04.101. [PubMed: 30998950]

(31). Tomita M; Munetsuna H; Sato T; Adachi T; Hino R; Hayashi M; Shimizu K; Nakamura N; Tamura T; Yoshizato K. Transgenic silkworms produce recombinant human type III procollagen in cocoons. Nat Biotechnol 2003, 21 (1), 52–6, DOI: 10.1038/nbt771. [PubMed: 12483223]

(32). Ogawa S; Tomita M; Shimizu K; Yoshizato K. Generation of a transgenic silkworm that secretes recombinant proteins in the sericin layer of cocoon: production of recombinant human serum

albumin. J Biotechnol 2007, 128 (3), 531–44, DOI: 10.1016/j.jbiotec.2006.10.019. [PubMed: 17166611]

(33). Wang F; Wang R; Wang Y; Zhao P; Xia Q. Large-scale production of bioactive recombinant human acidic fibroblast growth factor in transgenic silkworm cocoons. Scientific reports 2015, 5, 16323, DOI: 10.1038/srep16323. [PubMed: 26567460]

(34). Tada M; Tatematsu K; Ishii-Watabe A; Harazono A; Takakura D; Hashii N; Sezutsu H; Kawasaki N. Characterization of anti-CD20 monoclonal antibody produced by transgenic silkworms (Bombyx mori). MAbs 2015, 7 (6), 1138–50, DOI: 10.1080/19420862.2015.1078054. [PubMed: 26261057]

(35). Iizuka M; Ogawa S; Takeuchi A; Nakakita S; Kubo Y; Miyawaki Y; Hirabayashi J; Tomita M. Production of a recombinant mouse monoclonal antibody in transgenic silkworm cocoons. FEBS J 2009, 276 (20), 5806–20, DOI: 10.1111/j.1742-4658.2009.07262.x. [PubMed: 19740109]

(36). Wang Y; Wang F; Xu S; Wang R; Chen W; Hou K; Tian C; Wang F; Yu L; Lu Z; Zhao P; Xia Q. Genetically engineered bi-functional silk material with improved cell proliferation and anti-inflammatory activity for medical application. Acta Biomater 2019, 86, 148–157, DOI: 10.1016/j.actbio.2018.12.036. [PubMed: 30586645]

(37). Wang F; Hou K; Chen W; Wang Y; Wang R; Tian C; Xu S; Ji Y; Yang Q; Zhao P; Yu L; Lu Z; Zhang H; Li F; Wang H; He B; Kaplan DL; Xia Q. Transgenic PDGF-BB/sericin hydrogel supports for cell proliferation and osteogenic differentiation. Biomaterials Science 2020, 8 (2), 657–672, DOI: 10.1039/C9BM01478K. [PubMed: 31769455]

(38). Hino R; Tomita M; Yoshizato K. The generation of germline transgenic silkworms for the production of biologically active recombinant fusion proteins of fibroin and human basic fibroblast growth factor. Biomaterials 2006, 27 (33), 5715–24, DOI: S0142-9612(06)00652-1 [pii] 10.1016/j.biomaterials.2006.07.028. [PubMed: 16905183]

(39). Hu X; Shmelev K; Sun L; Gil ES; Park SH; Cebe P; Kaplan DL Regulation of silk material structure by temperature-controlled water vapor annealing. Biomacromolecules 2011, 12 (5), 1686–96, DOI: 10.1021/bm200062a. [PubMed: 21425769]

(40). Guo C; Li C; Vu HV; Hanna P; Lechtig A; Qiu Y; Mu X; Ling S; Nazarian A; Lin SJ; Kaplan DL Thermoplastic moulding of regenerated silk. Nat Mater 2020, 19 (1), 102–108, DOI: 10.1038/s41563-019-0560-8. [PubMed: 31844276]

(41). Lu Q; Hu X; Wang X; Kluge JA; Lu S; Cebe P; Kaplan DL Water-insoluble silk films with silk I structure. Acta Biomater 2010, 6 (4), 1380–7, DOI: 10.1016/j.actbio.2009.10.041. [PubMed: 19874919]

(42). Rockwood DN; Preda RC; Yucel T; Wang X; Lovett ML; Kaplan DL Materials fabrication from Bombyx mori silk fibroin. Nat Protoc 2011, 6 (10), 1612–31, DOI: 10.1038/nprot.2011.379 nprot.2011.379 [pii]. [PubMed: 21959241]

(43). Wang Q; Chen Q; Yang Y; Shao Z. Effect of various dissolution systems on the molecular weight of regenerated silk fibroin. Biomacromolecules 2013, 14 (1), 285–9, DOI: 10.1021/bm301741q. [PubMed: 23215147]

(44). Kim HJ; Kim MK; Lee KH; Nho SK; Han MS; Um IC Effect of degumming methods on structural characteristics and properties of regenerated silk. Int J Biol Macromol 2017, 104 (Pt A), 294–302, DOI: 10.1016/j.ijbiomac.2017.06.019. [PubMed: 28601646]

(45). Park BK; Um IC Effect of molecular weight on electro-spinning performance of regenerated silk. Int J Biol Macromol 2018, 106, 1166–1172, DOI: 10.1016/j.ijbiomac.2017.08.115. [PubMed: 28847607]

(46). Boulet-Audet M; Vollrath F; Holland C. Identification and classification of silks using infrared spectroscopy. J Exp Biol 2015, 218 (19), 3138–3149, DOI: 10.1242/jeb.128306. [PubMed: 26347557]

(47). Qi C; Xu L; Deng Y; Wang G; Wang Z; Wang L. Sericin hydrogels promote skin wound healing with effective regeneration of hair follicles and sebaceous glands after complete loss of epidermis and dermis. Biomater Sci 2018, 6 (11), 2859–2870, DOI: 10.1039/c8bm00934a. [PubMed: 30259043]

(48). Meinel L; Hofmann S; Karageorgiou V; Kirker-Head C; McCool J; Gronowicz G; Zichner L; Langer R; Vunjak-Novakovic G; Kaplan DL The inflammatory responses to silk films in vitro

and in vivo. Biomaterials 2005, 26 (2), 147–55, DOI: 10.1016/j.biomaterials.2004.02.047 S0142961204001589 [pii]. [PubMed: 15207461]

(49). Panilaitis B; Altman GH; Chen J; Jin HJ; Karageorgiou V; Kaplan DL Macrophage responses to silk. Biomaterials 2003, 24 (18), 3079–85, DOI: S0142961203001583 [pii]. [PubMed: 12895580]

(50). Saxena RK; Vallyathan V; Lewis DM Evidence for lipopolysaccharide-induced differentiation of RAW264.7 murine macrophage cell line into dendritic like cells. J Biosci 2003, 28 (1), 129–34, DOI: 10.1007/bf02970143. [PubMed: 12682436]

(51). Nazarov R; Jin HJ; Kaplan DL Porous 3-D scaffolds from regenerated silk fibroin. Biomacromolecules 2004, 5 (3), 718–26, DOI: 10.1021/bm034327e. [PubMed: 15132652]

(52). Yu YM; Arora A; Min WX; Roifman CM; Grunebaum E. EdU incorporation is an alternative non-radioactive assay to [H-3]thymidine uptake for in vitro measurement of mice T-cell proliferations. J Immunol Methods 2009, 350 (1–2), 29–35, DOI: 10.1016/j.jim.2009.07.008. [PubMed: 19647746]

(53). Tsubouchi K; Igarashi Y; Takasu Y; Yamada H. Sericin enhances attachment of cultured human skin fibroblasts. Biosci Biotechnol Biochem 2005, 69 (2), 403–5, DOI: JST.JSTAGE/bbb/69.403 [pii] 10.1271/bbb.69.403. [PubMed: 15725668]

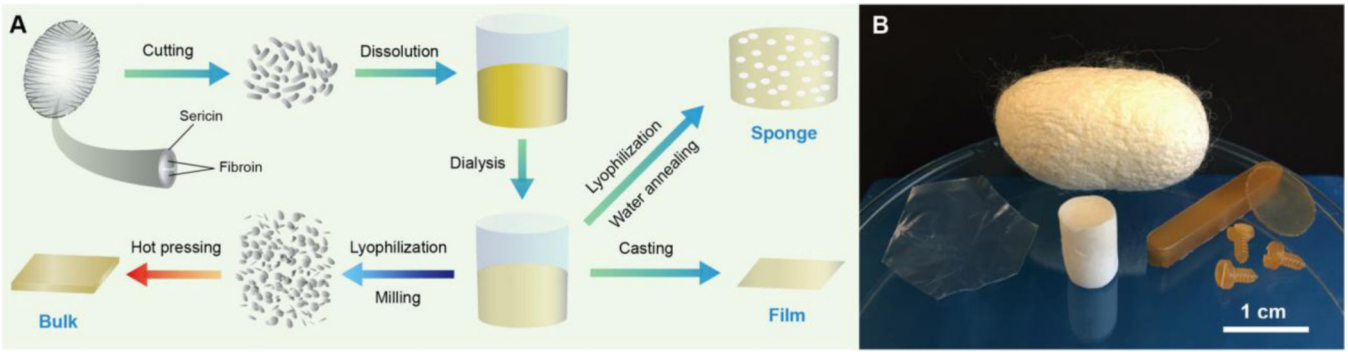

Fig. 1.

Schematic representation for generating biomaterials with whole raw cocoons. (A) Overall schematic of approach: 1) dissolving raw silk fibers to obtain regenerated aqueous SS-SF solution; 2) aqueous SS-SF solution-derived processing methods to fabricate SS-SF films and sponges; 3) thermoplastic molding of SS-SF in the solid state to directly form bulk materials and devices. (B) Photographs of films, sponges, bulk materials (e.g. bars, discs) and devices after machining (e.g. bone screws). Scale bar 1 cm.

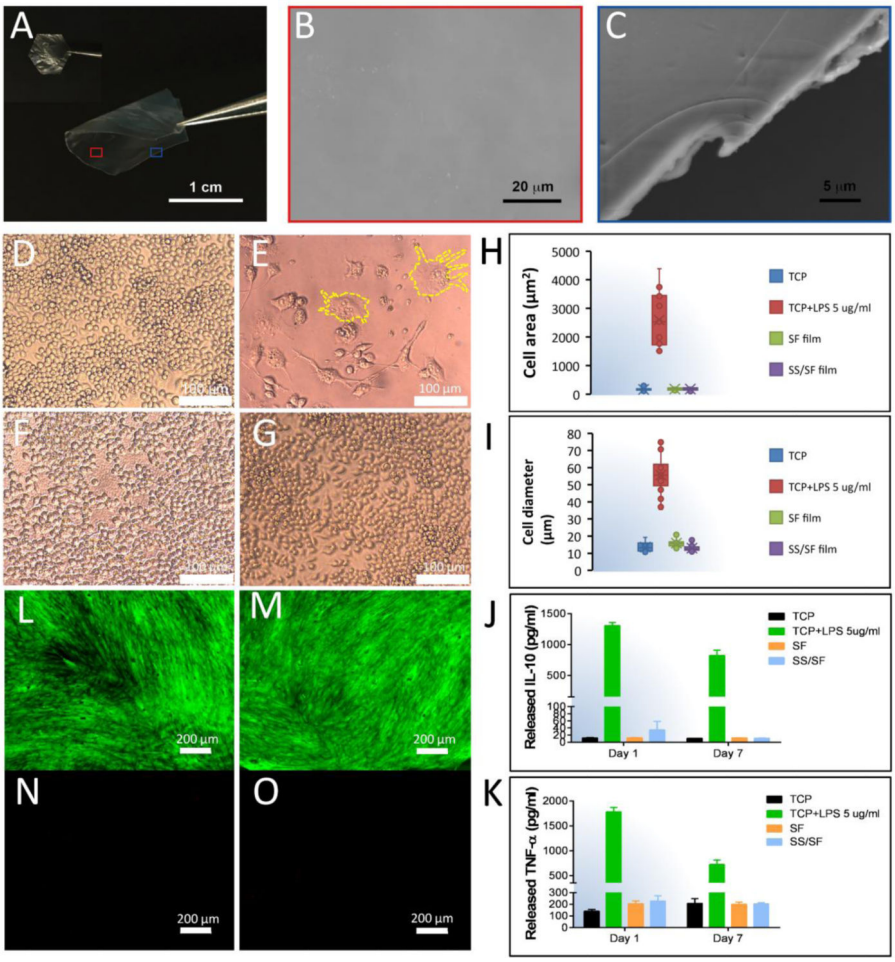

Fig. 2.

Characteristics of SS-SF films. (A) Photograph of SS-SF films under normal and bending conditions. Scale bar 1 cm. Surface (B) and cross section (C) SEM images of the SS-SF films, corresponding to the red and blue regions in (A), respectively. Scale bars for (B) and (C) 20 μm and 5 μm, respectively. Optical microscope images of macrophage RAW 264.7 cells grown on TCP plates (D), TCP plates with LPS (E), silk fibroin films (F) and SS-SF films (G) at day 1. Scale bar 100 μm. Cell areas (H) and diameters (I) calculations of RAW 264.7 cells grew on different substrates at day 1. Released inflammatory factors IL-10 (J) and TNF-α (K) from the RAW264.7 cells in media grown on different substrates at days 1 and 7. Viability of human fibroblast BJ cells growing on TCP plates (L and N) and the SS-SF films (M and O) at day 3 by Dead/Live staining. Live cells stained by Calcein-AM dye by green fluorescence (ex/em ~495 nm/~515 nm). Dead cells stained by EthD-1 dye and emitted red fluorescence (ex/em ~495 nm/~635 nm). Scale bar 200 μm.

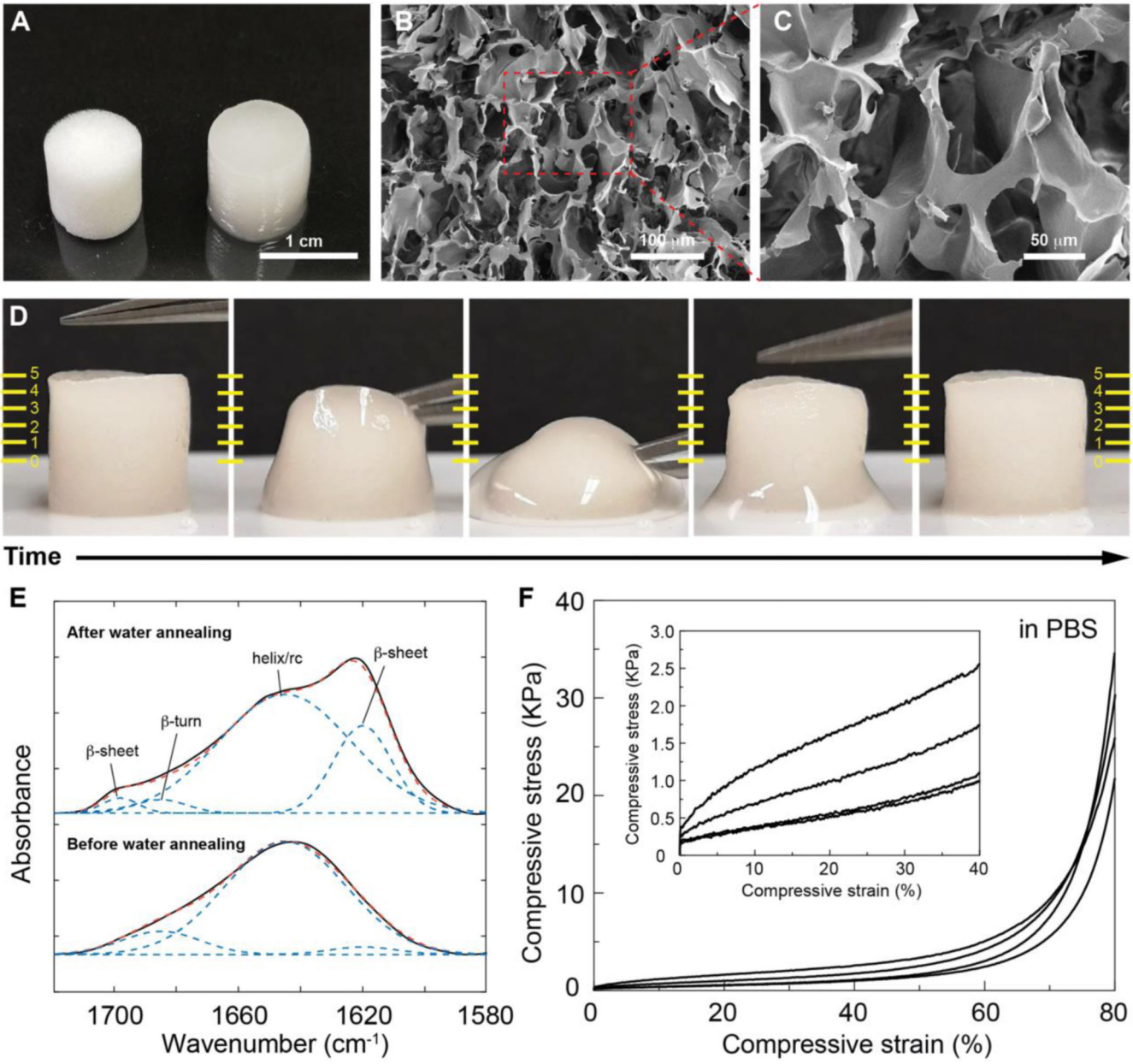

Fig. 3.

Physical properties of the SS-SF sponges. (A) Photographs of the 2% (w/v) SS-SF sponges in dry (left) and hydrated (right) states. (B-C) SEM of the 2% (w/v) SS-SF sponges at 300-fold and 1000-fold magnification, respectively. (D) Photograph showing compression cycle - of the SS-SF sponge in PBS. Scale bar 5 mm. (E) FTIR of the SS-SF sponge before (bottom inset) and after (top inset) water annealing. (F) Mechanical properties of the SS-SF sponges in hydrated conditions by compression test. Inset represents the maximum compressive stress and compressive modulus of the SS-SF sponges.

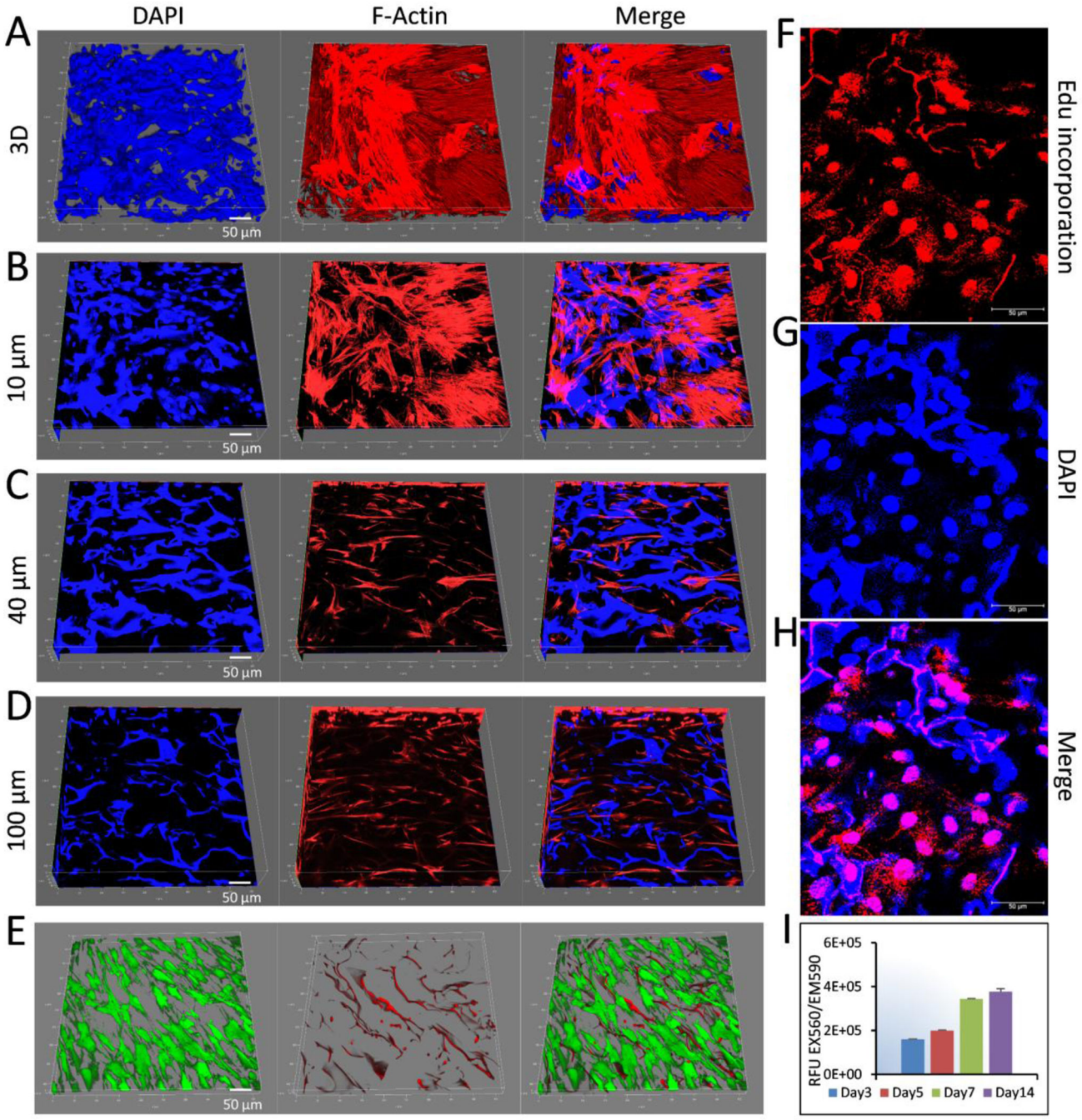

Fig. 4.

In vitro assessment of biological properties of the SS-SF sponges. (A) 3D Confocal scanning of MSCs grown for two weeks. Sponges stained with rhodamine-phalloidin for actin filaments (Red) and DAPI for nuclei (Blue), respectively. Images taken 100 μm in depth from top of the sponge. (B-D) Confocal microscopy of MSCs at 10, 40, and 100 μm depth of the SS-SF sponges, respectively. (E) Dead/Live staining and confocal microscopy of MSCs at week 2. (F-H) Edu incorporation reflecting cell proliferation of MSCs at week 2, where cells in f proliferation showed RFP fluorescent signals. Cell nuclei stained by DAPI (blue).

Scale bars for (A-H) represent 50 μm, respectively. (I) AlarmarBlue assay to monitor cell viability of MSCs in the SS-SF sponges for two weeks. Fluorescence intensities quantified using a fluorescence plate reader (ex/em ~560 nm/~590 nm). Measurements in triplicate and repeated independently four times.

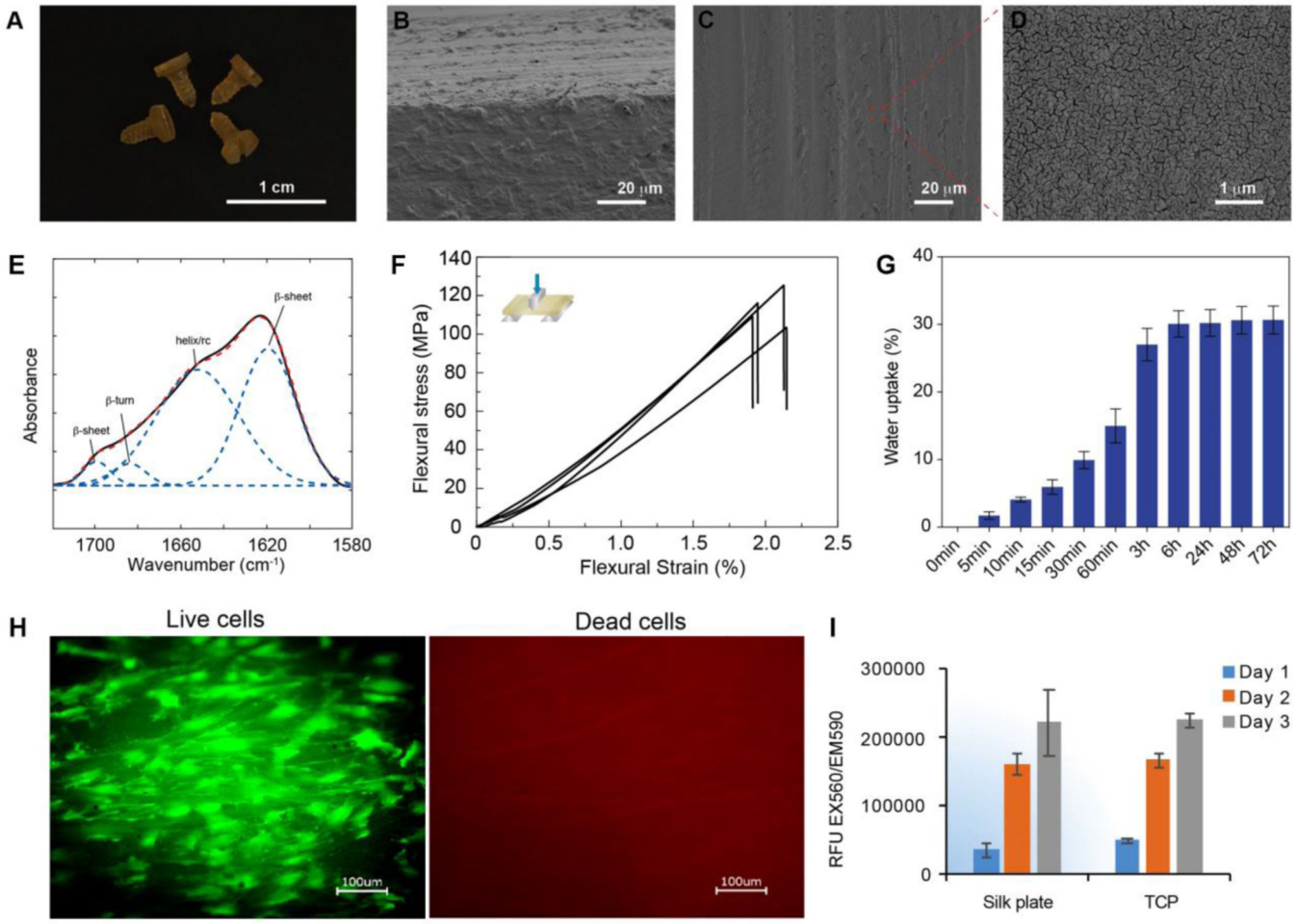

Fig. 5.

SS-SF based bulk materials and device fabrication (screws, plates). (A) Photograph of SS-SF bone screws. Scale bar 1 cm. (B-D) SEM images of bone screws. (E) FTIR characterization of bone screws. (F) Three-point bending curves for plates. (G) In vitro water uptake in PBS of the bone screws. (H) Dead/Live staining of MSCs grown on the plates. Scale bar 100 μm. (I) AlarmarBlue assay of the MSCs viability on the plates for three days. Fluorescence intensities quantified using a fluorescence plate reader (ex/em ~560 nm/~590 nm). Measurements in triplicate and repeated independently four times.